PCCP

PAPER

View Article Online
View Journal

Cite this: DOI: 10.1039/d3cp00691c

Predicting liquid–liquid phase separation in ternary organic–organic–water mixtures†

Noora Hyttinen

Received 13th February 2023,
Accepted 24th March 2023

DOI: 10.1039/d3cp00691c

rsc.li/pccp

Liquid–liquid phase separation (LLPS) affects the water uptake of aerosol particles in the atmosphere through Kelvin and Raoult effects. This study investigates LLPS in ternary mixtures containing water and two organic compounds, using a conductor-like screening model for real solvents (COSMO-RS). COSMO-RS found LLPS in all of the studied mixtures containing water and proxies for primary and secondary organic aerosol (POA and SOA, respectively), due to the limited solubility of the hydrophobic POA proxies in water. The computations predict additional three-phase states in some of the SOA–POA–water mixtures at relative humidity (RH) close to 100%, which was not observed in experiments, likely due to the relatively low RH (90%) used in the experiments. A computational method, such as COSMO-RS, allows for the estimation of new information on mixing states and mixtures that cannot be accessed experimentally. Comparison with experiments can also provide insight into which types of compounds may be present in SOA. Additionally, the possibility of LLPS can be assessed faster with rough estimates rather than by computing the whole phase diagram.

1 Introduction

The morphology of aerosol particles influences the gas-to-particle partitioning of both organic compounds and water. Knowledge on the phase behavior of aerosol particles is therefore important in the modeling of aerosol formation and cloud activation. The formation of multiple phases in a particle affects cloud activation through surface tension and water activity. In particles with a core–shell morphology, the organic-rich phase is often at the surface due to the surface tensions at the interfaces.[1] Organic compounds have a lower surface tension than water, indicating increased cloud activation in phase separated particles compared to one-phase particles, according to the Kelvin effect.[2,3] On the other hand, cloud activation is dependent on the water activity in the particle, following the Raoult effect. Ovadnevaite *et al.*[2] showed that the Kelvin effect from decreased surface tension has a larger effect in decreasing cloud activation supersaturation than the reduced Raoult effect from liquid–liquid phase separation (LLPS) in atmospheric aerosol particles. LLPS is therefore expected to increase cloud activation.

Water activity is generally lower in concentrated solutions than in dilute solutions, due to differences in water concentrations. However, phase separated organic–water mixtures strongly deviate from ideality. Water activity can even be close to unity in the equilibrium of binary two-phase states, while in one-phase mixed states with equal water content, water activity can be significantly lower.[4] If the particles contain multiple organic species with different polarities, phase separation can occur at relatively low relative humidities (water activities).[5]

LLPS in aerosol particles is highly dependent on the size of the particle.[6–11] Experiments have shown that smaller aerosol particles (specific size depending on the mixture) are homogeneous, while larger particles with the same composition have phase separated.[12] This indicates that a higher relative humidity (RH) is needed for smaller particles to phase separate compared to larger particles or bulk solutions, in cases where a high RH leads to phase separation.

In recent years, LLPS has been observed in particles containing one or more different organic compounds.[5,13–20] For example, Mahrt *et al.* investigated particles containing proxies of primary and secondary organic aerosol (POA and SOA, respectively) under varying RH conditions. They found that the particles phase separate at all RH if the oxygen-to-carbon ratio of the POA proxy is low enough (O : C $<$ 0.11).[5] Additionally, Mahrt *et al.* found that SOA–POA particles phase separate if the difference in the oxygen-to-carbon ratios (O : C) of the POA (single compound) and SOA (mixture of volatile organic compound oxidation products) is higher than 0.265.[20] Recently, three liquid phases were observed in aerosol particles consisting of water, inorganic salt and two organic species with different polarities.[21]

Department of Chemistry, Nanoscience Center, University of Jyväskylä, FI-40014 Jyväskylä, Finland. E-mail: noora.x.hyttinen@jyu.fi

† Electronic supplementary information (ESI) available: Comparing COSMO*therm* calculations with experiments; and table detailing the LLPS behavior of all studied mixtures. See DOI: https://doi.org/10.1039/d3cp00691c

Experimentally, it is not possible to investigate the phase separation behavior of real atmospheric aerosols with known compositions. Models are therefore necessary for estimating the phase behavior of atmospheric aerosols. Thermodynamic models, such as conductor-like screening model for real solvents (COSMO-RS[22–24]) and Aerosol Inorganic–Organic Mixtures Functional groups Activity Coefficients (AIOMFAC[25–27]), can be used to estimate the equilibrium liquid-phase compositions of mixtures. Both models are used for bulk liquid solutions, which makes them optimal for modeling LLPS in larger aerosol particles. COSMO-RS, implemented in the COSMO*therm* program,[28] has been shown to accurately estimate condensed-phase properties, such as solubilities and activity coefficients, of atmospherically relevant multifunctional compounds and water, if suitable conformer distributions are used in the calculation.[29–31]

Here, COSMO*therm* was used to calculate the phase diagrams of some of the ternary SOA–POA–water mixtures, investigated experimentally by Mahrt *et al.*[5] Additionally, the phase separation behavior was predicted for a large set of SOA–POA–water mixtures with possible SOA constituents ($p_{sat} < 10^{-5}$ Pa), as well as POA proxies with relatively high O : C ratios (O : C $\geq$ 0.125). The SOA constituents were selected from previous studies that have identified possible oxidation products of α-pinene, Δ3-carene, cyclohexene and isoprene.[4,32–34]

2 Computational methods

The COSMO-RS model,[22–24] implemented in the COSMO*therm* program,[28] was used for activity coefficient and liquid–liquid equilibrium (LLE) calculations. Activity coefficients are computed in COSMO*therm* using the following equation:

$$\ln \gamma_i(x) = \frac{\mu_i^*(x) - \mu_i^{*,\circ}(x^\circ, T, P)}{RT} \quad (1)$$

where x is the mixing state in mole fraction, T is the temperature (here 296 K), R is the gas constant (kJ K^{-1} mol^{-1}, when μ^* is given in kJ mol^{-1}) and $P = 10^5$ Pa is the reference pressure. Pseudo-chemical potential[35] μ_i^* is an auxiliary quantity defined using the chemical potential at the reference state μ°:

$$\mu_i^*(x) = \mu_i^\circ(x^\circ, T, P) + RT \ln \gamma_i(x) \quad (2)$$

The pure compound ($x_i = 1$) is used as the reference state composition x°. The use of pseudo-chemical potential allows for the calculation of activity coefficient in infinitely diluted states ($x_i \to 0$).

Phase equilibrium calculations are based on activity coefficients. At LLE, the LLE condition applies for all compounds i in the mixture:

$$a_i^\alpha(x^\alpha) = a_i^\beta(x^\beta) \quad (3)$$

Here α and β are the two liquid phases of the system and activity $a_i(x) = \gamma_i(x)x_i$. It should be noted that this calculation only finds the LLE and not whether the compounds are in solid or liquid form in the mixture. Estimating solid-liquid equilibria (SLE) requires experimental free energy of fusion of the solid component, which are not available for most of the studied SOA constituents. Additionally, COSMO*therm* finds LLE only for two liquid phases, and the existence of liquid–liquid–liquid equilibrium needs to be determined using multiple LLE calculations at different mixing states.

In COSMO*therm* LLE calculations, the accuracy threshold is by default 10^{-5}. The number of iteration points in the LLE calculations was increased to 100 000, because the LLE was not found for all mixtures in the default 1000 iteration points.

2.1 Input files for COSMO*therm* calculations

Conformer selection has a large effect on condensed-phase thermodynamic property calculations in COSMO*therm*.[30,36] Selecting conformers for COSMO*therm* calculations based on the number of intramolecular H-bonds gives the best agreement with experimental aqueous solubilities and activity coefficients of multifunctional carboxylic acids.[30] In solvent water, the number of intramolecular H-bonds correlates with the pseudo-chemical potential.[37] However, the calculated mixtures contain non-polar organic compounds and the most favorable conformers may not be the same in polar and non-polar solutions. Here, the conformers for COSMO*therm* calculations were therefore selected using their pseudo-chemical potentials, instead of their intramolecular H-bonding. Using pseudo-chemical potentials for conformer selection is applicable for all solvents and not just water. Additionally, ranking conformers based on their intramolecular H-bonding only works for compounds that contain H-bond donating functional groups, while using pseudo-chemical potentials allows the differentiation for all types of molecules.

All conformers were found using the systematic conformer sampling and Merck molecular force field (MMFF94[38]) of Spartan20.[39] For compounds that have more than 200 conformers, a subset of conformers were selected for further calculations based on their pseudo-chemical potentials in infinite dilution in water and water-insoluble organic matter (WIOM, CC(=O)C1OC2OC(OC2(C)O1)C1=CC(C)=CC(C)=C1[40]). The pseudo-chemical potentials were predicted using a machine learning model.[37,41] 200 lowest pseudo-chemical potential conformers in each of the two solvents (at most 400 conformers) were selected for density functional theory calculations using the COSMO*conf* program.[42,43]

The COSMO*conf* calculations included single-point calculations at the BP/SV(P) level of theory, followed by removal of conformers with similar pseudo-chemical potentials in a set of commonly used solvents. The geometries of all conformers were then optimized at the BP/SV(P) and BP/def-TZVP levels of theory with duplicate removal after both optimization steps based on both geometries and pseudo-chemical potentials. The input files for COSMO*therm* calculations were obtained through BP/def2-TZVPD-FINE level of theory single-point calculations. The input files of cyclohexene and isoprene oxidation products were taken directly from Hyttinen *et al.*[44,45]

In order to find the 10 most stable condensed-phase conformers (5 in both water and WIOM) for the thermodynamic property calculations, the pseudo-chemical potential of each

conformer was calculated using the BP_TZVPD_FINE_21 parametrization of COSMO*therm*. Additionally, only conformers within 2 kcal mol^{-1} from the lowest pseudo-chemical potential were selected. This ensures that unfavorable conformers are not included when the compound has very few conformers, as COSMO*therm* tends to favor low COSMO-energy conformers even if their pseudo-chemical potential in the solution is high.[30]

3 Results and discussion

Mahrt *et al.*[5] observed LLPS under all of their experimental RH conditions (<5%, 45% and 90%) in SOA–POA particles with a POA proxy O : C ratio below 0.11. Here, all selected POA proxies have O : C ratios higher than 0.11. Mahrt *et al.*[5] observed two phases in many mixtures containing octanol (O : C = 0.125), dioctyl phthalate (DOP; O : C = 0.166) and diethyl sebacate (DES; O : C = 0.29) especially at a high RH.[5] Additionally, DOP was an outlier in the experimental set of POA proxies, with LLPS occurring in more mixtures than the other POA proxies with relatively high O : C ratios.[5] In addition to octanol, diethyl sebacate and dioctyl phthalate, a water insoluble organic matter (WIOM; O : C = 0.33), commonly used in COSMO*therm* calculations, was selected as an additional POA proxy.

3.1 Comparison with particle experiments

Little experimental physicochemical property data of atmospheric multifunctional compounds are available in the literature. Comparisons between COSMO*therm*-derived phase-equilibrium calculations and experiments of atmospherically relevant binary mixtures show that COSMO*therm* is able to predict experimental solubilities, when the lowest pseudo-chemical potential conformers of the compounds are used in the calculations (see Section S1 of the ESI†).

Mahrt *et al.*[5] reported LLPS in ternary mixtures with known organic : organic mass ratios (1 : 1) under three different RH conditions: dry (<5%), 45% and 90%. There were three distinct cases in the ternary SOA–POA–water mixtures:

1. Phase separation occurring at all RH, *e.g.*, glycerol–DES.
2. Phase separation occurring at relatively low RH (<90%), *e.g.*, maleic acid–DES and *cis*-pinonic acid–DOP.
3. No LLPS at RH below 90%, *e.g.*, *cis*-pinonic acid–DES.

Here, COSMO*therm* calculations are compared with the phase separation behavior of the three example cases using the COSMO*therm*-computed water activities (and LLE) in mixing states with varying water contents.

For the first case, Mahrt *et al.*[5] observed LLPS in glycerol–DES particles in both dry and humid conditions. COSMO*therm* calculations predict phase-separation in all water contents, see Fig. 1. All of the experimental mixtures (1 : 1 organic mass ratio, dashed black line) fall into the unstable region, indicating LLPS into one phase containing water and glycerol, and a DES-rich phase that contains only small amounts of water and glycerol.

For the second case, Fig. 2 shows the calculated ternary phase diagram of the maleic acid–DES–water mixture. The

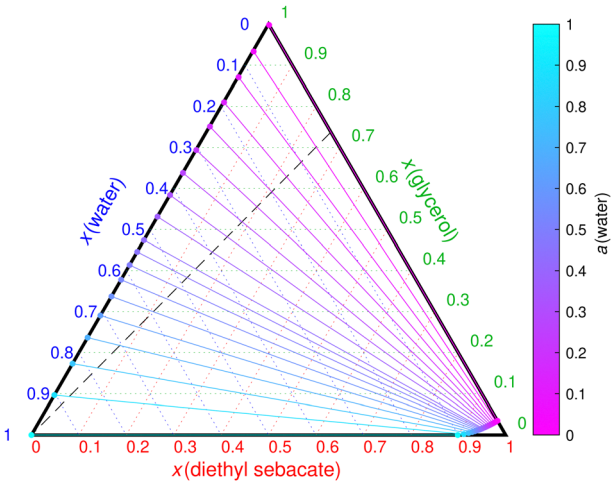

Fig. 1 COSMO*therm*-derived phase diagram of glycerol, diethyl sebacate and water at 296 K. The solid lines represent tie lines, where the color is water activity in both liquid phases (solid circles) at phase separation. The dashed line represents the 1 : 1 glycerol-to-diethyl sebacate mass ratio of the experiments of Mahrt *et al.*[5]

calculations agree with the experimental observations of one phase at 45% RH and two phases at 90% RH. COSMO*therm*-predicted phase separation RH is around 75% for the experimental 1 : 1 mass ratio of the two organics. An additional crystal phase was seen in the experiments under dry conditions (RH <5%), which is likely caused by maleic acid being a solid at 296 K. However, the solid solubility of maleic acid was not investigated further in this study.

For the third case, Mahrt *et al.*[5] observed no phase separation in the *cis*-pinonic acid–DES particles. On the other hand, LLPS was observed at high RH (90%) in the *cis*-pinonic acid–DOP

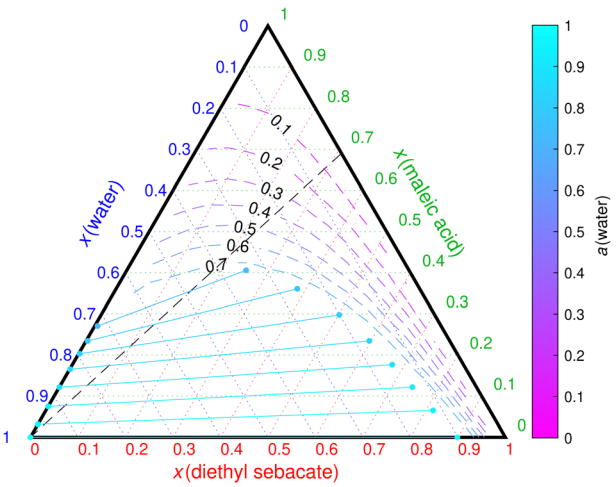

Fig. 2 COSMO*therm*-derived phase diagram of the ternary maleic acid–diethyl sebacate–water mixture at 296 K. Solid lines represent tie lines. The dashed contour lines represent water activity in a one-phase state and are derived from individual points calculated in different mixing ratios. The dashed black line represents the 1 : 1 mass ratio of maleic acid and diethyl sebacate used in the experiments of Mahrt *et al.*[5] Note that maleic acid is solid at 296 K and its aqueous solubility is around 0.1 mole fraction.[46]

particles,[5] corresponding to the second case. Fig. 3(a) and (b) show COSMO*therm*-derived liquid-phase diagrams of the ternary aqueous mixtures containing DES and DOP, respectively.

In the *cis*-pinonic acid–DES–water mixture, an almost pure aqueous phase is formed at close to 99% RH (Fig. 3(a)). The *cis*-pinonic acid–DES particle would therefore not take up enough water in the experimental RH of 90% to result in LLPS. This is in agreement with the experiments.[5]

In the *cis*-pinonic acid–DOP–water mixture, COSMO*therm* predicts an additional phase separation into two phases, both containing significant amounts of all three components. The water activity at the tie line with the lowest water mole fraction found by COSMO*therm* is 0.41. This is in agreement with the experiments,[5] where two phases were observed at 90% RH in particles containing DOP but not DES. Even though Mahrt *et al.*[5] did not observe LLPS at 45% RH, the small size of the particles and uncertainties of COSMO*therm* calculations may explain why a higher RH was needed for LLPS in the experiments than what is predicted by COSMO*therm*.

COSMO*therm* found additional LLE (dotted lines in Fig. 3(b)), where the binodal compositions fulfill the LLE conditions, but the binodal compositions are inside the other phase separation region (empty markers in Fig. 3(b)). These compositions are likely in the metastable region, which may become relevant in smaller particles. Additionally, the solid lines form a triangle, marking a 3-phase region. This was not seen in the experiments with up to 90% RH. A higher RH (close to 100%) would likely be required to reach high enough water content in the particles to form an additional water-rich phase predicted by COSMO*therm*.

With the exception of the *cis*-pinonic acid–DOP–water mixture, there is a clear correlation between phase separation in the three binary mixtures of the ternary mixture and the RH required for phase separation in the ternary mixtures. For example, when LLE is found between the two organic compounds (in addition to one of the organic compounds and water), the mixture phase separates at all RH (Fig. 1). On the other hand, if both organic phases separate with water, water activity is likely to be very high at phase separation and RH close to 100% is needed for LLPS (Fig. 3(a)). If one of the organic compounds is miscible with both water and the other organic, the LLPS RH is more likely to be below 95% (Fig. 2).

3.2 Estimating LLPS from infinite dilution activity coefficients

Finding ternary LLPS using COSMO*therm* is very time consuming, because a large number of activity coefficient calculations are needed to locate pairs of mixing states that fulfill the LLE condition of eqn (3). Similarly, the LLE in binary solutions requires tens to thousands of activity coefficient calculations, depending on how strongly the mixture deviates from ideality. The solubility of a solute i in a solvent s (when solubility is low) can be estimated as the inverse of the activity coefficient of the solute in the infinite dilution in the solvent ($x^s_{sol} = 1/\gamma_i^s$). This estimate can be used as a tool to screen a large number of compounds with a single activity coefficient calculation.

Fig. 4 shows how the infinite dilution activity coefficients of the studied SOA constituents correlate with the phase separation behavior of the ternary mixtures. The cases similar to the *cis*-pinonic acid–DOP–water mixture (*i.e.*, the existence of a second phase separation region) were identified by a single LLE calculation at SOA : POA:water mixing ratio of 0.3 : 0.4 : 0.3.

The green markers represent mixtures that phase separate at all RH. In general, the binary SOA–POA mixtures phase separate and most of the water will partition to the SOA-rich phase. On the other hand, the mixtures that require a high RH to phase separate (blue markers in Fig. 4) contain SOA that phase separates with water. In these solutions, water forms its own phase, while the POA and SOA form one organic-rich phase that also contains water. The intermediate cases (magenta markers in Fig. 4) that phase separate at RH between 1 and 98% contain

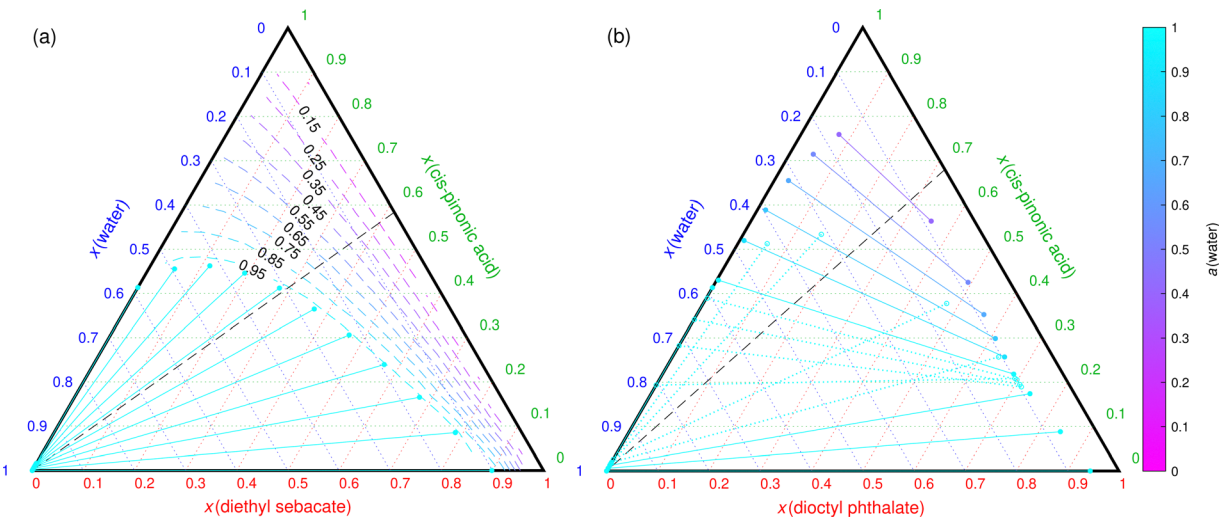

Fig. 3 COSMO*therm*-derived phase diagram of *cis*-pinonic acid, water and (a) diethyl sebacate and (b) dioctyl phthalate at 296 K. The dashed black line represents the 1 : 1 mass ratio of the organic species in the particle experiments of Mahrt *et al.*[5] Solid lines represent tie lines (two-phase states) and the dashed colored lines represent water activity in one-phase states. Tie lines where one or both of the phase compositions are inside another phase separation region are marked with dotted lines and empty markers.

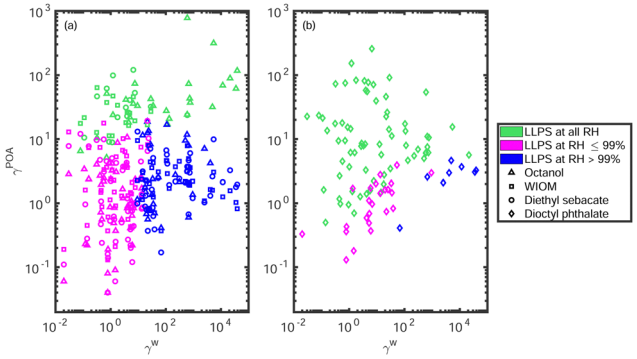

Fig. 4 Classification of LLPS based on activity coefficients in the infinite dilution in water (γ^{w}) and POA (γ^{POA}). Different POA are distinguished by markers and colors represent predicted phase behaviors in the SOA–POA–water mixture at equilibrium.

SOA that does not phase separate with water or POA. Both phases will contain significant amounts of all 3 components. It should be noted that the SOA : POA mixing ratio affects the LLPS behavior of the particle. For example, "LLPS at all RH" means that there exists some SOA : POA mixing ratio region, in which the binary SOA–POA mixture phase separates into two liquid phases.

Table S1 of the ESI† summarizes the types of LLPS behaviors of all of the studied ternary mixtures. Several mixtures that are predicted to form three liquid phases at RH close to 100% were also identified. Three phases can form, when all of the three constituents are partially miscible with the other two constituents. Additionally, there exist mixtures similar to *cis*-pinonic acid–DOP–water, where three phases were predicted, even though full miscibility was predicted between *cis*-pinonic acid and DOP (Fig. 3(b)).

3.3 POA comparison

All of the studied POA proxies phase separate with water at 296 K. Additionally, the POA proxy does not affect phase separation in the binary SOA–water mixture. The differences in the LLPS behavior between POA proxies must therefore arise from the SOA–POA interaction. Many of the studied SOA constituents phase separate with some of the studied POA proxies but are miscible with others. These differences can be determined with binary SOA–POA LLE calculations or estimated with the infinite dilution activity coefficients.

Octanol, WIOM and DES (Fig. 4(a)) present similar phase behavior in relation to the SOA activity coefficients in infinite dilution in water and POA, while the mixtures containing DOP are likely to phase separate with relatively low γ_{SOA}^{POA} values (Fig. 4(b)). Chemically DES and DOP are quite similar compounds, as they have identical oxygen containing functional groups. However, DOP contains a benzene ring and longer alkyl groups than DES. Still, COSMO*therm* predicts LLPS in the SOA–DOP mixture with much lower SOA activity coefficients ($\gamma_{SOA}^{DOP} \sim 1$) compared to the corresponding SOA–DES mixtures ($\gamma_{SOA}^{DES} \sim 10$). These results explain why two phases were observed in more mixtures containing DOP than other POA proxies with similar O : C ratios.[5] The main difference between DOP and the other studied POA proxies is the higher tendency of DOP to phase separate even when the infinite dilution activity coefficients are relatively low (high solubility).

Generally, if LLPS exists in the binary SOA–water and POA–water mixtures, the ternary mixture phase separates at RH close to 100%. Additional phase separations are mainly predicted for DOP as the POA proxy as well as some mixtures containing WIOM and DES, when the SOA constituent is large (molar mass > 290 g mol^{-1}). Three-phase mixtures are predicted for all four POA proxies, when all three binary pairs of the ternary mixture phase separate.

Fig. 5 shows phase diagrams of caronic acid–POA–water mixtures with the four studied POA proxies. Caronic acid is an example SOA constituent, that exhibits the same LLPS behavior (0% < LLPS RH < 99%) with the four POA proxies. However, the predicted phase separation RH is much higher for mixtures containing DES, octanol and WIOM (above 90%; Fig. 5(a), (c) and (d), respectively) than DOP (RH < 35%; Fig. 5(b)). The lower LLPS RH of the caronic acid–DOP–water mixture is caused by caronic acid partitioning more to the aqueous phase than the DOP-rich phase, especially at high caronic acid mole fractions. Additionally, the aqueous phase in the caronic acid–WIOM–water mixture contains more caronic acid than the equivalent aqueous phases in the mixtures containing DES and octanol. Unfortunately, the differences in LLPS RH cannot be easily determined with binary LLE calculations, and the full ternary phase diagrams need to be computed to obtain this information.

3.4 SOA comparison

The phase separation behavior of organic compounds has previously been explained with the O : C ratios of the compounds.[5,47] With COSMO*therm* calculations, it is possible to differentiate between structural isomers of the same elemental composition. There is no clear similarity among the LLPS behavior of the different isomers of the same elemental compositions. This suggests that there are significant differences between the oxygen containing functional groups and the position of the functional groups in the organic compounds.

For example, previous COSMO*therm* calculations showed that the interaction between water and the different isomers (*trans*-β, *cis*-β, δ_1, δ_4) of isoprene epoxydiol (IEPOX; $C_5H_{10}O_3$) is similar.[4] However, the addition of a POA proxy (WIOM or DES) to the mixture leads to different phase behavior between the different IEPOX isomers. *Cis*- and *trans*-β-IEPOX have limited solubilities in WIOM and DES, while δ_1- and δ_4-IEPOX are miscible with both WIOM and DES. Fig. 6(a) and (b) show phase diagrams of WIOM, water and δ_1- and *cis*-β-IEPOX, respectively. The LLPS RH of the δ_1-IEPOX–WIOM–water mixture is around 30%, while *cis*-β-IEPOX–WIOM–water particles phase separate at all RH.

Compared to the glycerol–DES–water mixture, a significant amount of WIOM mixes in the aqueous SOA-rich phase of the IEPOX–WIOM–water mixtures. Additionally, the WIOM-rich phase in the δ_1-IEPOX–WIOM–water mixture (Fig. 6(a))

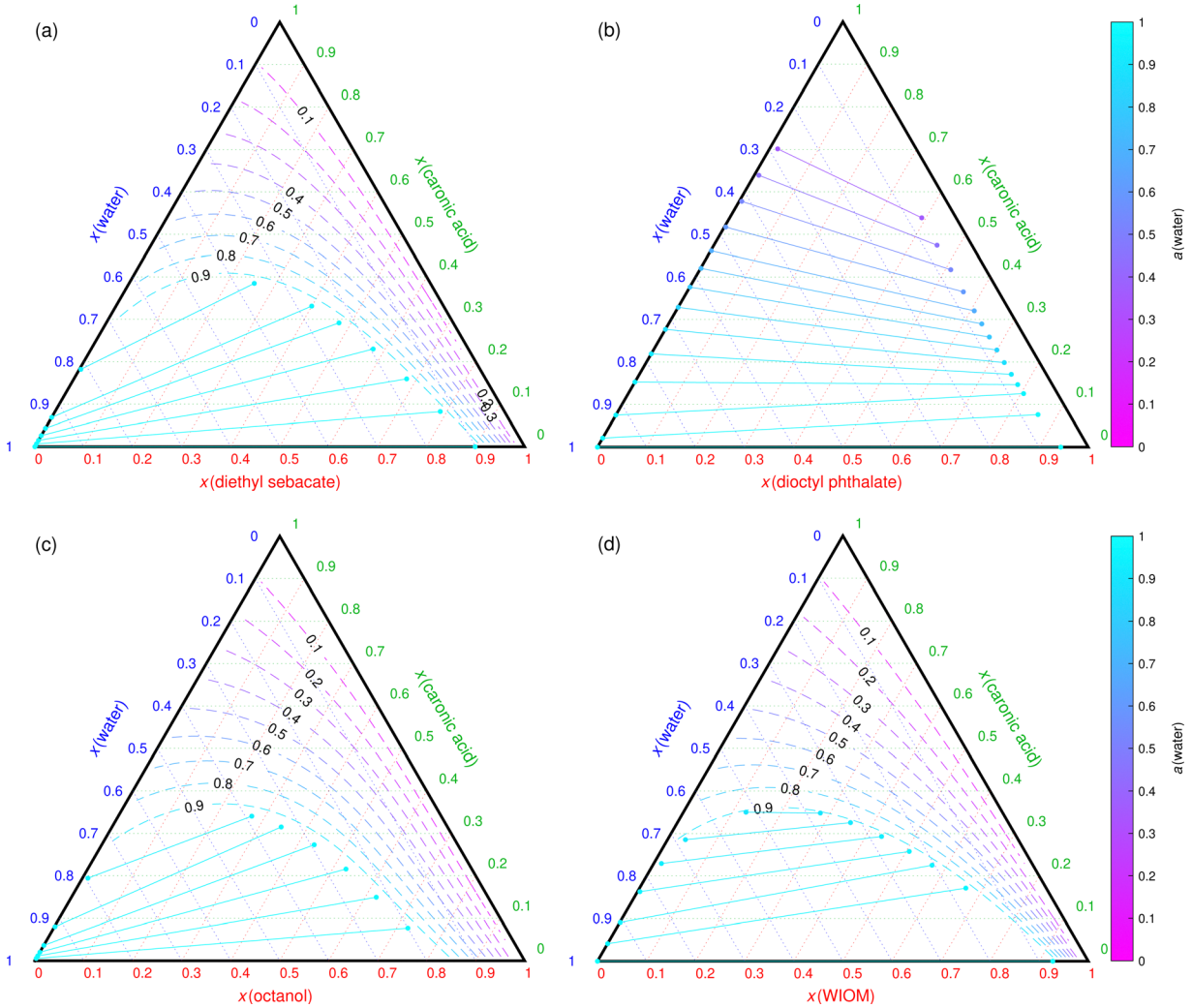

Fig. 5 COSMO*therm*-derived phase diagrams of ternary caronic acid, water and (a) diethyl sebacate, (b) dioctyl phthalate, (c) octanol and (d) WIOM mixtures at 296 K. Solid lines represent tie lines (two-phase states) and the dashed colored lines represent water activity in one-phase states.

contains 0.07–0.12 mole fraction of water. In this case, adding δ_1-IEPOX to the mixture enhances the solubility of water in the WIOM-rich phase compared to the binary WIOM–water mixture. *Cis*-β-IEPOX has the opposite effect, worsening the solubility of water in the WIOM-rich phase.

In general, compounds containing more than 11 carbon atoms are more likely to phase separate with either water or POA. This indicates that large SOA constituents form particles that have LLPS behavior independent of the RH (see Table S1 of the ESI†). Instead, the large SOA constituents form one-phase mixtures under RH < 100% more often than the smaller SOA constituents.

3.5 Ternary SOA–SOA–water mixtures

Experiments have shown that α-pinene + O_3 SOA particles phase separate at high RH (>95%, case 3), but no LLPS was observed in α-pinene + OH SOA particles (miscibility).[14,17] The lack of LLPS at low RH indicates that the SOA constituents mix well together. In addition, the second liquid phase forming at high RH is likely an aqueous phase. This corresponds to a SOA–POA–water mixture where the SOA constituent and the POA proxy phase separate with water in the binary mixture (Fig. 3(a)). These experimental results agree with COSMO*therm* calculations, which predict miscibility between all binary mixtures of the studied SOA constituents, and the limited water solubility of some α-pinene + O_3 oxidation products.

Mahrt *et al.*[47] found that a SOA–SOA particle phase separates, when the difference in the average O : C ratios, Δ(O : C), of the two SOA is equal to or higher than 0.47, while two SOA with similar O : C (Δ(O : C) < 0.47) form one-phase particles. No RH dependence was observed in these experiments, corresponding to the glycerol–DES–water mixture. Two phases were observed in particles containing oxidation products of one sesquiterpene with a low O : C ratio (valencene, β-caryophyllene, farnesene) and one aromatic compound with a high O : C ratio (toluene, catechol). All of the combinations containing α-pinene ozonolysis products formed one-phase particles.[47]

The O : C ratio of the studied SOA constituents ranges from 0.26 to 1.2. COSMO*therm* predicts miscibility between most pairs of the studied SOA constituents, regardless of their O : C ratios. An exception is glycerol, which phase separates with

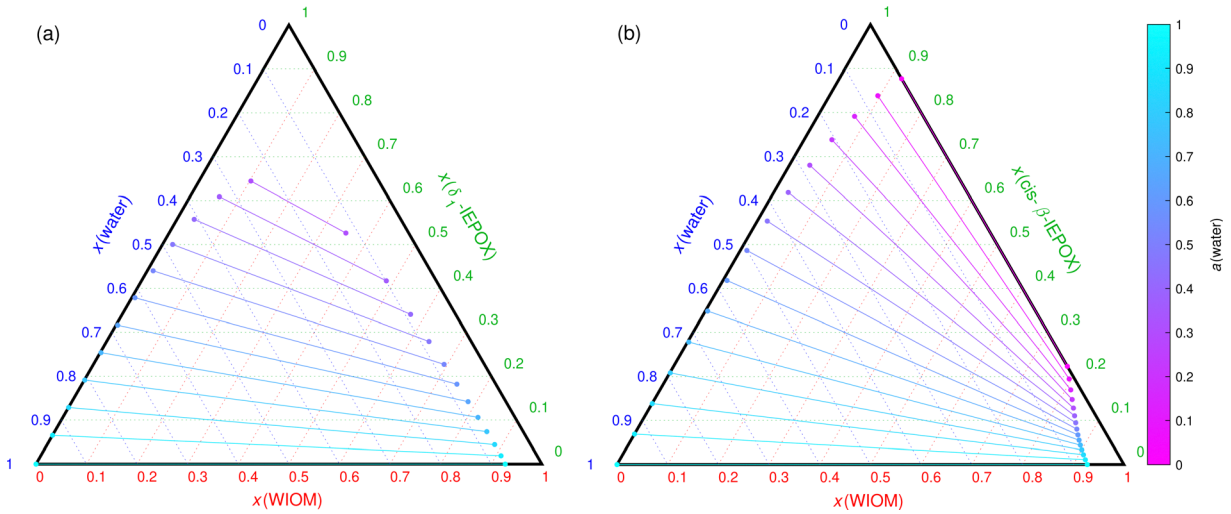

Fig. 6 COSMO*therm*-derived phase diagrams of (a) δ_1-IEPOX and (b) *cis*-β-IEPOX, WIOM and water at 296 K. The lines represent tie lines (two-phase states) of the mixtures.

some isomers of the larger studied SOA constituents, C_{12} and C_{18} compounds with O : C ratios between 0.33 and 1.17. The Δ(O : C) values of these phase separating binary mixtures range from 0 to 0.67. Fig. 7 shows the phase diagram of glycerol–$C_{18}H_{26}O_6$–water mixture (Δ(O : C) = 0.67). Here, water is more soluble in the SOA constituent than any of the POA proxies. This leads to a smaller two-phase region compared to the glycerol–DES–water mixture (Fig. 1). The occurrence of LLPS is therefore more dependent on the SOA : SOA mixing ratio compared to SOA : POA mixing ratios.

As was hypothesized by Mahrt *et al.*[47] the actual range of O : C ratios of each SOA likely plays a role in the phase state of SOA–SOA particles. Unfortunately, only the average O : C ratios of SOA are available from experiments.[47] Perhaps the SOA from some aromatic precursors (high average O : C) contains compounds that are similar to glycerol (and water). These compounds could separate from other highly oxygenated SOA constituents even under dry conditions and form phase separated particles under all RH conditions. Or possibly some oxidation products of sesquiterpenes are similar to the POA proxies (low O : C and hydrophobic), while having low enough volatilities to remain in the particle phase (high molar mass).

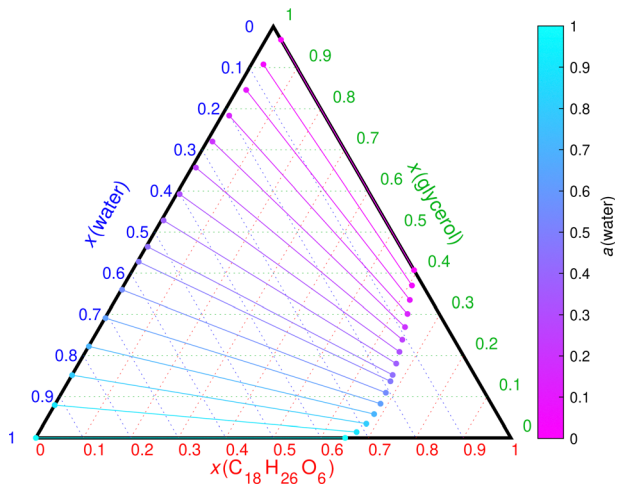

Fig. 7 COSMO*therm*-derived phase diagram of glycerol, $C_{18}H_{26}O_6$ (CC1(C)C(CC═O)CC1C(═O)OC(═O)CC1CC(C(O)═O)C1(C)C) and water at 296 K. The lines represent tie lines (two-phase states) of the mixture.

4 Conclusions

Information on phase behavior of aerosol particles is needed for climate models. LLPS affects the water uptake and CCN activation of atmospheric aerosol through, among other things, surface tension and water activity. In SOA–POA–water mixtures, water activity coefficient is likely to be above unity ($\gamma > 1$) in all one-phase states that contain significant amounts of POA. This is seen from the contour lines of the phase diagrams (Fig. 2, 3(a) and 5(a), (c), and (d)). However, SOA–water mixtures may be close to ideal solutions, if the SOA constituent and water are miscible (*e.g.*, binary IEPOX–water solutions[4]).

At LLPS, water activity may be below ideality (enhanced water uptake), if the SOA-rich phase contains only small amounts of POA, as is the case in the glycerol–DES–water mixture (Fig. 1). Even in the *cis*-β-IEPOX–WIOM–water mixture, the activity coefficients of water at phase separation (aqueous phase) are slightly above unity for all of the computed tie-lines. Based on calculations presented here, POA lowers water uptake into aerosol particles. Water uptake is only enhanced (in terms of decreased water activity) by LLPS in SOA–POA aerosol particles, when the SOA-rich phase contains very little POA ($x_{POA} < 0.001$).

Aerosol process models that consider LLPS through lowered surface tension of a hydrophobic organic shell phase and the non-ideality of water have been able to explain experimental hygroscopic growth better than models that assume one-phase particles.[3] Additionally, when the water content of the particle is high enough at equilibrium under high RH conditions, the

particle becomes mixed, leading to a surface tension equal to that of pure water.[3] In these aqueous particles, the enhancing effect of the lower surface tension on water uptake is lost. However, some of the low surface tension organics may still act as surfactants and partition to the particle–air interface of one-phase particles.

Based on comparisons between COSMO*therm* calculations and experiments, COSMO*therm* is able to predict experimental phase equilibria in binary and ternary supermicron particles. The calculated results complement experimental data on LLPS to improve the description of different SOA and POA types in atmospheric models. In order to further validate the accuracy of COSMO*therm* in LLPS calculations, more measurements are needed under different RH conditions using a range of organic mixing ratios.

Data availability

Cosmo-files used in the COSMO*therm* calculations can be accessed through Jyväskylä University Digital Repository (JYX) at: **https://doi.org/10.17011/jyx/dataset/86223**.[48]

Conflicts of interest

There are no conflicts to declare.

Acknowledgements

I thank Dr Silvia Calderón for our inspiring discussions on thermodynamics. The Academy of Finland, Grant No. 338171, is gratefully acknowledged for the financial contribution, and the CSC - IT Center for Science, Finland, for computational resources.

References

1 N.-O. Kwamena, J. Buajarern and J. Reid, *J. Phys. Chem. A*, 2010, **114**, 5787–5795.
2 J. Ovadnevaite, A. Zuend, A. Laaksonen, K. J. Sanchez, G. Roberts, D. Ceburnis, S. Decesari, M. Rinaldi, N. Hodas, M. C. Facchini, J. H. Seinfeld and C. O'Dowd, *Nature*, 2017, **546**, 637–641.
3 P. Liu, M. Song, T. Zhao, S. S. Gunthe, S. Ham, Y. He, Y. M. Qin, Z. Gong, J. C. Amorim, A. K. Bertram and S. T. Martin, *Nat. Commun.*, 2018, **9**, 4076.
4 N. Hyttinen, J. Elm, J. Malila, S. M. Calderón and N. L. Prisle, *Atmos. Chem. Phys.*, 2020, **20**, 5679–5696.
5 F. Mahrt, E. Newman, Y. Huang, M. Ammann and A. K. Bertram, *Environ. Sci. Technol.*, 2021, **55**, 12202–12214.
6 D. P. Veghte, D. R. Bittner and M. A. Freedman, *Anal. Chem.*, 2014, **86**, 2436–2442.
7 M. A. Freedman, *Acc. Chem. Res.*, 2020, **53**, 1102–1110.
8 M. B. Altaf, A. Zuend and M. A. Freedman, *Chem. Commun.*, 2016, **52**, 9220–9223.
9 T. M. Kucinski, J. N. Dawson and M. A. Freedman, *J. Phys. Chem. Lett.*, 2019, **10**, 6915–6920.
10 P. E. Ohno, Y. Qin, J. Ye, J. Wang, A. K. Bertram and S. T. Martin, *ACS Earth Space Chem.*, 2021, **5**, 1223–1232.
11 T. M. Kucinski, E.-J. E. Ott and M. A. Freedman, *J. Phys. Chem. A*, 2021, **125**, 4446–4453.
12 D. P. Veghte, M. B. Altaf and M. A. Freedman, *J. Am. Chem. Soc.*, 2013, **135**, 16046–16049.
13 M. Song, C. Marcolli, U. Krieger, A. Zuend and T. Peter, *Geophys. Res. Lett.*, 2012, **39**, L19801.
14 L. Renbaum-Wolff, M. Song, C. Marcolli, Y. Zhang, P. F. Liu, J. W. Grayson, F. M. Geiger, S. T. Martin and A. K. Bertram, *Atmos. Chem. Phys.*, 2016, **16**, 7969–7979.
15 K. Gorkowski, N. M. Donahue and R. C. Sullivan, *Environ. Sci. Technol.*, 2017, **51**, 12154–12163.
16 M. Song, S. Ham, R. J. Andrews, Y. You and A. K. Bertram, *Atmos. Chem. Phys.*, 2018, **18**, 12075–12084.
17 S. Ham, Z. B. Babar, J. B. Lee, H.-J. Lim and M. Song, *Atmos. Chem. Phys.*, 2019, **19**, 9321–9331.
18 E.-J. E. Ott, E. C. Tackman and M. A. Freedman, *ACS Earth Space Chem.*, 2020, **4**, 591–601.
19 K. Gorkowski, N. M. Donahue and R. C. Sullivan, *Chem*, 2020, **6**, 204–220.
20 F. Mahrt, Y. Huang, J. Zaks, A. Devi, L. Peng, P. E. Ohno, Y. M. Qin, S. T. Martin, M. Ammann and A. K. Bertram, *Environ. Sci. Technol.*, 2022, **56**, 3960–3973.
21 Y. Huang, F. Mahrt, S. Xu, M. Shiraiwa, A. Zuend and A. K. Bertram, *Proc. Natl. Acad. Sci. U. S. A.*, 2021, **118**, e2102512118.
22 A. Klamt, *J. Phys. Chem.*, 1995, **99**, 2224–2235.
23 A. Klamt, V. Jonas, T. Bürger and J. C. W. Lohrenz, *J. Phys. Chem. A*, 1998, **102**, 5074–5085.
24 F. Eckert and A. Klamt, *AIChE J.*, 2002, **48**, 369–385.
25 A. Zuend, C. Marcolli, B. P. Luo and T. Peter, *Atmos. Chem. Phys.*, 2008, **8**, 4559–4593.
26 A. Zuend, C. Marcolli, A. M. Booth, D. M. Lienhard, V. Soonsin, U. K. Krieger, D. O. Topping, G. McFiggans, T. Peter and J. H. Seinfeld, *Atmos. Chem. Phys.*, 2011, **11**, 9155–9206.
27 G. Ganbavale, A. Zuend, C. Marcolli and T. Peter, *Atmos. Chem. Phys.*, 2015, **15**, 447–493.
28 *BIOVIA COSMOtherm, Release 2021*, Dassault Systèmes, **https://www.3ds.com**, 2021.
29 G. Michailoudi, N. Hyttinen, T. Kurtén and N. L. Prisle, *J. Phys. Chem. A*, 2020, **124**, 430–443.
30 N. Hyttinen and N. L. Prisle, *J. Phys. Chem. A*, 2020, **124**, 4801–4812.
31 N. Hyttinen, R. Heshmatnezhad, J. Elm, T. Kurtén and N. L. Prisle, *Atmos. Chem. Phys.*, 2020, **20**, 13131–13143.
32 N. Hyttinen, M. Wolf, M. P. Rissanen, M. Ehn, O. Peräkylä, T. Kurtén and N. L. Prisle, *J. Phys. Chem. A*, 2021, **125**, 3726–3738.
33 D. Thomsen, J. Elm, B. Rosati, J. T. Skønager, M. Bilde and M. Glasius, *ACS Earth Space Chem.*, 2021, **5**, 632–644.
34 N. Hyttinen, I. Pullinen, A. Nissinen, S. Schobesberger, A. Virtanen and T. Yli-Juuti, *Atmos. Chem. Phys.*, 2022, **22**, 1195–1208.

35 A. Ben-Naim, *Solvation Thermodynamics*, Plenum Press, New York and London, 1987.
36 T. Salthammer, S. Grimme, M. Stahn, U. Hohm and W.-U. Palm, *Environ. Sci. Technol.*, 2022, **56**, 379–391.
37 N. Hyttinen, A. Pihlajamäki and H. Häkkinen, *J. Phys. Chem. Lett.*, 2022, **13**, 9928–9933.
38 T. A. Halgren, *J. Comput. Chem.*, 1996, **17**, 490–519.
39 *Spartan'20*, *Wavefunction Inc.*, *Irvine, CA*, 2020.
40 M. Kalberer, D. Paulsen, M. Sax, M. Steinbacher, J. Dommen, A. S. Prévôt, R. Fisseha, E. Weingartner, V. Frankevich, R. Zenobi and U. Baltensperger, *Science*, 2004, **303**, 1659–1662.
41 N. Hyttinen, *JYX Digital Repository*, Version 1, 2022, DOI: **10.17011/jyx/dataset/83604**.
42 *BIOVIA COSMOconf 2021*, *Dassault Systèmes*. **https://www.3ds.com**, 2021.
43 *TURBOMOLE, a development of University of Karlsruhe and Forschungszentrum Karlsruhe GmbH, Version 7.4.1*, *TURBOMOLE GmbH*, 2010.
44 N. Hyttinen, M. Wolf, M. P. Rissanen, M. Ehn, O. Peräkylä, T. Kurtén and N. L. Prisle, *Zenodo*, Version 1, 2021, DOI: **10.5281/zenodo.4291305**.
45 N. Hyttinen, J. Elm, J. Malila, S. M. Calderón and N. L. Prisle, *Zenodo*, Version 1, 2019, DOI: **10.5281/zenodo.3552309**.
46 A. Apelblat and E. Manzurola, *J. Chem. Thermodyn.*, 1987, **19**, 317–320.
47 F. Mahrt, L. Peng, J. Zaks, Y. Huang, P. E. Ohno, N. R. Smith, F. K. A. Gregson, Y. Qin, C. L. Faiola, S. T. Martin, S. A. Nizkorodov, M. Ammann and A. K. Bertram, *Atmos. Chem. Phys.*, 2022, **22**, 13783–13796.
48 N. Hyttinen, *JYX Digital Repository*, Version 1, 2023, DOI: **10.17011/jyx/dataset/86223**.